Iron related solar cell instability: Imaging analysis and impact on cell performance

M.C. Schubert [a,*], M. Padilla [a], B. Michl [a], L. Mundt [a], J. Giesecke [a], J. Hohl-Ebinger [a], J. Benick [a], W. Warta [a], M. Tajima [b,1], A. Ogura [b]

[a] Fraunhofer Institute for Solar Energy Systems, Freiburg, Germany
[b] Meiji University, Kawasaki, Japan

ABSTRACT

Iron is an omnipresent and efficiency-limiting impurity in p-type silicon solar cells. A very useful technique to detect the interstitial iron concentration in boron doped silicon is based on carrier lifetime measurements at two metastable states of iron, namely interstitial and bound to boron. We present a further development of this technique which images the iron concentration not only on wafer level but also on finished solar cells and in this way enables the most direct access to the impact of interstitial iron on cell performance. With the help of this method we reveal that remaining iron in solar cells may be responsible for significantly unstable current–voltage characteristic under illumination. Recommendations for stable cell measurements even for cells containing a significant concentration of iron are given.

© 2015 Elsevier B.V. All rights reserved.

1. Introduction

Iron is one of the most relevant impurities in p-type silicon for solar cells [1,2]. Its role in mono- and multicrystalline solar cells has been intensively discussed (see e.g. [3–7]). The concentration as well as configuration of iron in a processed solar cell depend on initial concentration, details on crystallization and the solar cell process, (see e.g. [8–10]) as well as on the effectiveness of cleaning steps [11]. While iron may be detrimental in the form of precipitates, iron point defects even in concentrations in the order of 10^{10} cm^{-3} may limit the performance of high efficiency solar cells in the case of p-type silicon. A specific characteristic of interstitial iron in boron doped silicon is its tendency to pair with boron. The defect parameters of both states, Fe_i and FeB, differ such that injection dependent differences of the carrier lifetime can be measured and evaluated to a quantitative interstitial iron concentration [12,13]. This method has also been transferred to camera based photoluminescence imaging [14] where images of the interstitial iron distribution can be obtained on silicon wafers and bricks [15].

Since the state of the iron defect changes with illumination, its impact on cell properties depends on illumination and storage history. This leads to instabilities of the final cell parameters which may affect the outcome of performance measurements. As a result of both, iron being efficiency limiting and a source of instability, the detection of iron defects on cell level is of high relevance. Since previously lifetime measurements were mainly restricted to wafer level due to a hindering influence of the cell's metallization, test wafers without metallization need to be processed in order to avoid a problematic etch-off of the (typically fired) metallization layer before measurement.

Recently, spatially resolved carrier lifetime measurements on solar cells by dynamically calibrated Photoluminescence (PL) Imaging via modulated luminescence [16] were realized which, as we show in this work, enable the detection of interstitial iron by such lifetime measurements. The differences in measurements on passivated wafers, particularly due to the influence of surface recombination, are discussed.

From this data the dependence of cell parameters on illumination is quantitatively assessed. The example of a highly efficient cell structure shows that already very low concentrations of iron may cause cell efficiency measurements to vary by several percent

---

* Corresponding author.
 E-mail address: martin.schubert@ise.fraunhofer.de (M.C. Schubert).
 [1] Also with Institute of Space and Astronautical Science/JAXA, Sagamihara, Japan.

(relative) as a function of preceding illumination conditions of the cell under test. The analysis of interstitial iron in cells thus provides a useful means not only to study efficiency-limiting iron defects during cell processing but also to quantitatively determine current–voltage measurement uncertainties originating from iron.

2. Iron imaging on cells

2.1. Principle

Positively charged interstitial iron atoms in boron doped silicon tend to pair with negatively charged substitutional boron atoms via Coulomb attraction. Iron boron pairs are stable under dark conditions at room temperature but break with carrier injection (e.g. via illumination). The preparation of both states is well known and used for measurements of interstitial iron on wafer level [14,17] where lifetime measurements in both states are compared.

An obvious difference between iron measurements on cell compared to wafer level is that lifetime measurements are complicated by metal layers, enhanced surface recombination (in comparison to surface passivated wafers), and enhanced lateral conductivity due to highly conductive layers such as emitter and metal coating.

The recently developed method of dynamically calibrated lifetime images on solar cells [16] is suitable to measure effective carrier lifetime despite metallization layers. An initial result was reported in [18]. In the approach used in this work, a solar cell under test is illuminated by a monochromatic laser with a wavelength of 790 nm and the resulting photoluminescence signal is measured with the help of a photodiode. Carrier lifetime is deduced from the analysis of the retarded photoluminescence signal in a selfconsistent approach as described in [19]. In contrast to the original method which has been developed for wafers the photodiode is positioned in reflection mode rather than in transmission mode to overcome the opaqueness of the cell's metallization layer. Details of this adapted method are described in [16].

The lifetime measurements are performed under open circuit voltage. The effective lifetime obtained may be significantly affected by surface recombination at the metallized back side $S_{eff,back}$ and by carrier flows to the emitter region. The latter effect can be expressed by an effective front side surface recombination rate $S_{eff,front}$ whereas the PL signal from the emitter region can be neglected [20]. Neglecting radiative recombination and inhomogeneities of the carrier depth profile, the effective lifetime on cell level $\tau_{eff,cell}$ can be expressed as

$$\frac{1}{\tau_{eff,cell}} = \frac{1}{\tau_{Fei}} + \frac{1}{\tau_{FeB}} + \frac{1}{\tau_{SRH,other}} + \frac{1}{\tau_{Auger}} + U_{surf},\tag{1}$$

where τ_{Fei} and τ_{FeB} represent the Shockley–Read–Hall (SRH) lifetimes due to recombination via the Fe$_i$ and FeB defect levels, respectively, and $\tau_{SRH,other}$ is the corresponding lifetime due to SRH recombination via all other defects which may be present in the cell under test. U_{surf} is the recombination rate at the surfaces. For the simple case of homogeneous carrier profiles U_{surf} can be expressed by

$$U_{surf} = \frac{1}{\tau_{surf}(S_{eff,front})} + \frac{1}{\tau_{surf}(S_{eff,back})}\tag{2}$$

where τ_{surf} is the lifetime due to recombination at the surface (see e.g. [21,22]).

In many cases carrier (depth) profiles may be non-uniform in illuminated solar cells. For a more accurate solution also for inhomogeneous carrier profiles the simulations shown below in this work are considering surface recombination as boundary conditions for the carrier transport equations rather than switching to effective lifetime values. More recent details about the determination of surface recombination properties are reported in [23].

Since bulk recombination via SRH levels, recombination at surfaces and Auger recombination are injection dependent, care has to be taken when comparing two measurements of the effective lifetime. If the injection dependence of other SRH recombination processes and surface recombination is sufficiently weak then the iron concentration can be calculated in analogy to [14] by

$$\begin{aligned}\left[Fe_{i,cell}\right] &= C(\Delta n_{Fei}, \Delta n_{FeB}) \\ &\times \left(\frac{1}{\tau_{eff,cell,Fei}(\Delta n_{Fei})} - \frac{1}{\tau_{eff,cell,FeB}(\Delta n_{FeB})} - \frac{1}{\tau_{intrinsic}(\Delta n_{Fei})} \right. \\ &\left. + \frac{1}{\tau_{intrinsic}(\Delta n_{FeB})} \right).\end{aligned}\tag{3}$$

with

$$C(\Delta n_{Fei}, \Delta n_{FeB}) = \frac{1}{\chi^{Fe_i} - \chi^{FeB}},$$

$$\begin{aligned}\chi^{Fe_i} &= \frac{v_{th}(N_A + \Delta n_{Fei})}{\frac{1}{\sigma_n^{Fei}}\left(N_A + p_1^{Fei} + \Delta n_{Fei}\right) + \frac{\Delta n_{Fei}}{\sigma_p^{Fei}}}, \chi^{FeB} \\ &= \frac{v_{th}(N_A + \Delta n_{FeB})}{\frac{1}{\sigma_n^{FeB}}(N_A + \Delta n_{FeB}) + \frac{1}{\sigma_p^{FeB}}\left(n_1^{FeB} + \Delta n_{FeB}\right)}\end{aligned}$$

where $\tau_{eff,cell,Fei}$, $\tau_{eff,cell,FeB}$ and Δn_{Fei}, Δn_{FeB} are the effective carrier lifetime and the excess carrier density in the Fe$_i$ and FeB states, respectively. $\tau_{intrinsic}$ is the intrinsic lifetime due to Auger and radiative recombination [24], v_{th} is the thermal velocity, N_A is the concentration of acceptor atoms, and $\sigma_{n/p}^{Fei}$, $\sigma_{n/p}^{FeB}$ are the corresponding capture cross sections. p_1^{Fei} and n_1^{FeB} are the hole SRH densities for the Fe$_i$ state and the electron SRH densities for the FeB state, respectively.

The most critical point for the determination of the interstitial iron concentration on cell level is the inhomogeneous carrier depth profile during lifetime measurement which may affect the measurement because of the injection dependence of the iron defect recombination as well as because of reabsorption effects of the PL signal. The reason for the inhomogeneity is the strong influence of surface recombination on the carrier depth profile. For measurements on wafer level this problem can be overcome by using appropriate surface passivation layers (e.g. Al$_2$O$_3$ or SiN$_x$). Since surface recombination in cells is typically significant, systematic errors on the determined iron concentration may occur [25]. It is therefore necessary to quantify this effect in order to assess the need of implementing an appropriate correction function. For this purpose carrier densities as would be expected from a PL measurement are simulated as a function of iron concentration in both states, Fe$_i$ and FeB as outlined in the following.

For the simulation the carrier depth profile is calculated from the continuity equation under steady state conditions as a function of iron concentration in both cases, Fe$_i$ and FeB. The generation illumination wavelength has been assumed as 790 nm, as also realized in the experiment. An illumination intensity of 0.25 sun (6.4×10^{16} photons/(s cm^2)) was chosen. Recombination via Fe$_i$ and FeB defect levels, other (constant) SRH defect levels as well as intrinsic (Auger and radiative) recombination are considered. In the presented results a background lifetime of 1 ms has been assumed. Losses of excess carriers into the front and rear surface layers are implemented by cell specific effective surface recombination velocities which have been gained from PC1D simulations

on the basis of measured doping profiles, external quantum efficiency as well as open circuit voltage, and have been determined to be $S_{eff,front}=300$ cm/s and $S_{eff,back}=600$ cm/s. As in an experimental setup the detected PL intensity is due to luminescence events from all depths. The simulated PL result is consecutively obtained by integration of PL intensity over thickness, considering a pyramid surface texturing (via extended light paths due to diffraction according to Snell's law), reabsorption as well as the quantum efficiency of the measurement setup. From these calculations the expected iron concentration measurement result can be determined as a function of initial iron concentration in analogy to [25]. Since the measureable iron concentration is affected by potential systematic errors, a corresponding correction function can be calculated from these simulations according to Eq. (3) (see Fig. 1). Although the systematic errors are small for iron concentrations shown in this paper (i.e. iron concentrations in the order of 10^{11} cm^{-3}) using the modeled surface recombination values, errors may be significant for larger iron concentrations or larger front surface recombination. More details about the simulation of systematic errors in iron measurements are described in [25]. The corrected measured iron concentration is then obtained by

$$[Fe_{i,cell}]_{corr} = C_{sys} \times [Fe_{i,cell}]_{meas} \qquad (4)$$

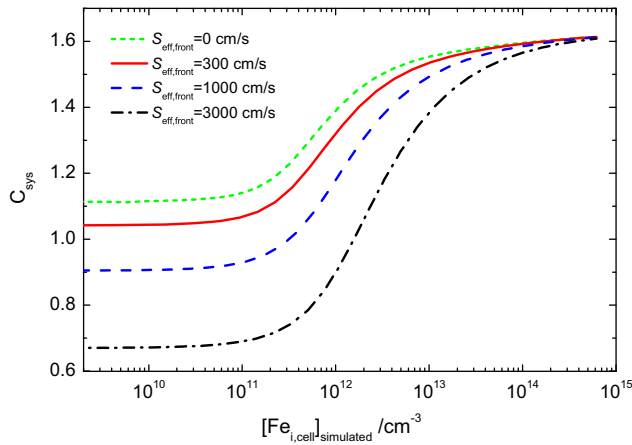**Fig. 1.** Correction function C_{sys} of systematic error in iron measurements as a function of simulated iron concentration which corresponds to the measureable iron concentration.

with the correction factor

$$C_{sys} = \frac{[Fe_{i,cell}]_{initial}}{[Fe_{i,cell}]_{simulated}}. \qquad (5)$$

Fig. 1 shows the correction factor as a function of iron concentration measured on cell level. The systematic error at $S_{eff,back}=600$ cm/s is low for sufficiently small interstitial iron concentrations and small front surface recombination velocities $S_{eff,front}$. Larger values of $S_{eff,front}$ lead to underestimation of the iron concentration, whereas high iron concentrations tend to be overestimated.

Note that the minimum systematic error for low iron concentration is not expected at negligible front side recombination, which is due to a balancing effect of the assumed rear side recombination. The role of surface recombination on the systematic error becomes less pronounced for high iron concentration, which reflects the high carrier recombination at iron defects in the bulk.

For iron analyses without spatial resolution a simplified procedure of the one described above can be applied: instead of deducing the carrier densities in both states from PL measurements V_{oc} measurements can also be converted to global carrier densities via

$$V_{oc} = \frac{kT}{q} \ln\left(\frac{n \cdot p}{n_i^2}\right) \qquad (6)$$

which converts to excess minority carrier density Δn with $n \cdot p = \Delta n \cdot N_A + \Delta n^2$ via

$$\Delta n = \frac{-N_A}{2} + \sqrt{\frac{N_A^2}{4} + n_i^2 \ \exp\left(\frac{qV_{oc}}{kT}\right)}. \qquad (7)$$

The calculated value for Δn is, strictly speaking, only valid at the pn-junction. It may, nevertheless, be used as a rough estimate for the depth-averaged carrier density and effective carrier lifetime via $\tau_{eff}=\Delta n/G$, G being the generation rate. The quality of this approximation depends on the exact value of the surface recombination velocity on the back side. Iron concentration can then be estimated globally as described above with Eqs. (3) and (4).

3. Experimental results

The experimental results have been obtained on 2×2 cm² p-type solar cells on 4 in. Float Zone silicon wafers with a resistivity of
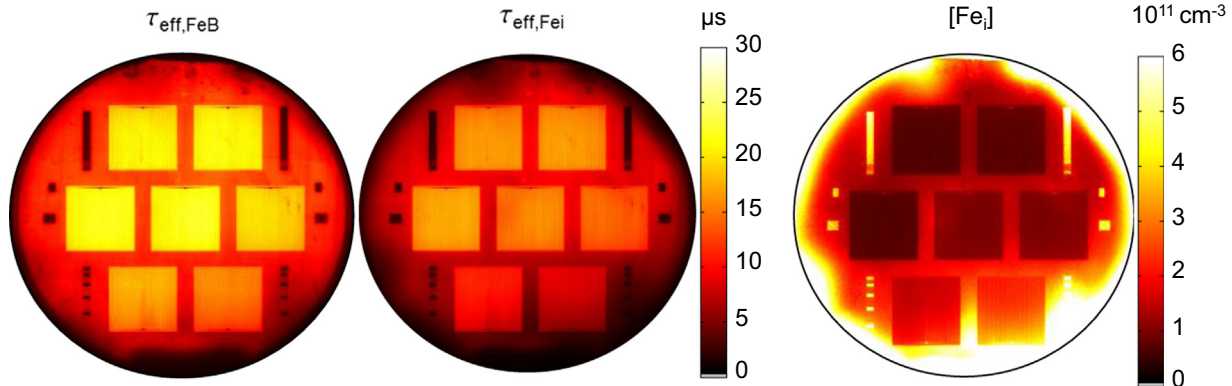

Fig. 2. Effective bulk lifetime on wafer with cells in the FeB state (left) and Fe$_i$ state (center) as well as calculated concentration of interstitial iron (right). Note that the calibration has been performed on cell area. The absolute values of carrier lifetime and iron concentration in areas between the cells are underestimated (respectively overestimated) because of the lower effective sample emissivity due to missing surface texture.

0.5 Ω cm. The front side of the cells featured a textured surface with a deeply driven-in 120 Ω/sq phosphorus doped emitter. The front side passivation was realized by a 105 nm thick thermally grown SiO_2 layer. The front side contacts of the cells consisted of an evaporated layer stack of Ti/Pd/Ag, the rear side of a full area boron doped BSF with a sheet resistance of 15 Ω/sq which was contacted by evaporated aluminum. Seven cells were processed on each wafer, which enables comparison with spatially resolved results on wafer level. Due to this lab type process untypically high concentration of iron (see below) attained efficiencies were limited to 18.1–20.1% in Fe_i state (18.4–20.4% in FeB state).

Fig. 2 shows images of the quantitative effective carrier lifetime from dynamically calibrated Photoluminescence Imaging. Please note that, since the calibration has been performed on the (textured) cell area, the carrier lifetime indicated on the wafers in between cells is underestimated because of lower emissivity of these areas (and have to be disregarded). Differences in reflectivity have been considered in the calibration procedure.

It is apparent from the images that the lifetime is different in both metastable states. In comparison with iron measurements on wafer level, the effective spatial resolution which can be expected from iron measurements on cell level is decreased due to enhanced lateral conductivity which is caused by the emitter layer and front side metallization of each cell.

From this data the intersitial iron concentration has been calculated and is also shown in Fig. 2. Again, the analysis of quantitative values is restricted to the calibrated cell areas. Interstitial iron concentrations in the order of 10^{11} cm^{-3} are apparent.

The comparison of the obtained results with appropriate reference measurement techniques is difficult given the low level of iron concentration. For this reason well-established Fe-imaging on wafer level [14] has been chosen to assess the new method. The cells were etched back after measurement, passivated with an ALD deposited Al_2O_3 surface layer and measured again for interstitial iron. The sample preparation, including temperature treatment above 400 °C in hydrogen containing environment, needed during sample processing may as well have an impact on the iron concentration and lead to differences in the quantitative measurement results. Still this is expected to be a good qualitative reference.

Fig. 3 summarizes the results of this comparison. For all samples the measured iron concentration on wafer level qualitatively follows the cell measurements on a 30–60% lower level, which indicates losses of dissolved iron during processing. It is probable that the passivation process reduced the interstitial iron concentration by low temperature internal gettering [26–28] (425° for 25 min). Hydrogen

which was introduced to some extent by the etch back and also during ALD deposition may also have passivated Fe point defects and might be responsible for a lower concentration of measured interstitial iron on wafer level [29,30].

Alternative explanations for the quantitative differences would be underestimated front surface recombination rates used in the calculation of the volume lifetimes for the cells which were extracted from cell modeling. For effective front side recombination velocity of the cells of $S_{eff,front}=5000$ cm/s agreement between cell and passivated wafer measurement (featuring negligible surface recombination) would be obtained (see Fig. 1). Finally, during etch-back of the cells, several micrometers of silicon are removed which might have contained a higher concentration of interstitial iron. However, the first alternative is considered implausible because such a high surface recombination velocity is not supported by the cell data (EQE, V_{oc}). For the latter explanation a questionably high iron concentration in the surface near layers of the p-type base of the solar cells would be needed.

4. Current–voltage instabilities caused by iron

Besides causing lifetime and therefore cell performance degradation, iron in solar cells can be problematic for the assessment of cell performance parameters: arbitrary illumination and storage in the dark may result in variations of the bulk lifetime and thus cell performance. Therefore, temperature and illumination history of a cell may influence cell results. Storage in the dark of a cell for several hours will lead to pairing of interstitial iron atoms with boron, fast (flash) measurements then result in higher performance compared to measurements after prolonged (steady state) illumination with sufficient intensity which will break FeB pairs.

Especially if calibrated cells are used as calibrated references where high stability as a function of time is crucial, it is necessary to follow a qualification procedure which allows one to safely identify any occurrence of an iron-related instability. First priority is then to exclude usage of such a cell as a reference. In case instability is encountered on a cell already in use, the procedure must allow one to assign the instability unambiguously to an iron contamination. Then reproducible measurement results can still be realized by a well-defined illumination procedure before measurement.

It is the aim of this chapter to quantify cell performance metastability as a function of iron concentration for the above presented cell type as an example. This shall give an indication for a maximum iron concentration associated with a tolerable metastability. Since carrier lifetime depends on carrier density which varies between open circuit, maximum power point, and short circuit conditions, the iron-related change of carrier lifetime influences open circuit voltage, fill factor, and short circuit current to a different degree. The actual dependence is influenced by the background recombination, iron concentration, cell concept, and illumination intensity and should be calculated specifically for a solar cell structure under test.

The presented cell structure may serve as a representative example: Fig. 4 shows the relative change of open circuit voltage, short circuit current, fill factor and efficiency as a function of iron concentration under standard test conditions (1 sun, AM1.5G spectrum). We assume a change of iron defects from a pure interstitial state to the state where all interstitial iron atoms are paired with boron. The PC1D-based simulations are compared with experimental results of obtained relative cell efficiency instability. For the simulation it has been assumed that the bulk carrier lifetime is dominated by recombination via the Fe_i and FeB defect. Defect parameters have been taken from [31,32]. The experimental data has been obtained by IV measurements of the cells under test in both iron states at room temperature. The FeB
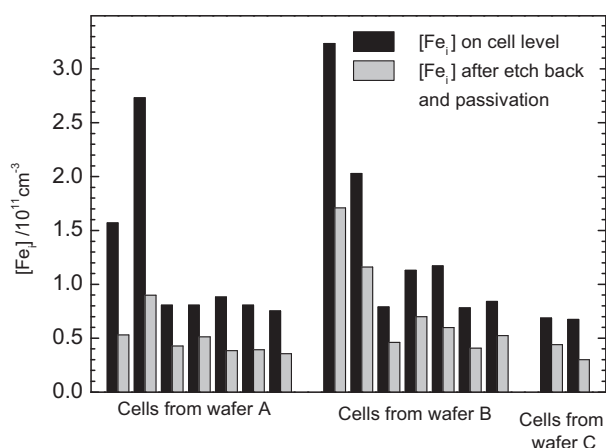

Fig. 3. Comparison of measurements of interstitial iron concentration on cell level (black) and wafer level after etch back of cells and subsequent surface passivation with ALD deposited Al_2O_3 (gray).

state (resulting in higher efficiencies) was induced by keeping the contacted solar cell in dark conditions on a temperature controlled measurement chuck at 70 °C for at least 20 min, followed by an IV measurement with a HALM Flasher after the cell cooled down to 25 °C. The Fe_i state was created by halogen light illumination of the cell for at least 10 min, followed by subsequent fast IV measurement at 25 °C. The measurement results are summarized in Table 1 and compared in Fig. 4 with simulations.

The comparison between measured iron concentration via the presented PLI approach and the estimated iron concentration from the V_{oc} instability shows reasonable agreement considering the expected measurement uncertainties apart from cell 2. The larger deviation is most probably due to unexpectedly low carrier lifetime which has been measured in this sample. The systematic deviation between both approaches was determined by linear fitting to only 8%. This observation supports the explanation of reduced iron concentration on wafers after etch back (Fig. 3).

Note that for Fig. 4 we chose to plot and compare the relative values of cell parameter variation rather than the absolute ones. This avoids on the one hand additional scattering due to processing influences on the cell's performance while on the other hand it enables a direct comparison of the magnitude of instability of each performance parameter.

The PC1D based simulation is in excellent agreement with the experimental values except for cell 2 and cell 4. Closer analysis of these cells reveals that the background lifetime, which is due to defects other than iron, is exceptionally low such that these cells are only partly limited by metastable iron defects. Consequently, the parameter instability is lower than that predicted by the simulation.

Both, simulation and experiment show an increasing instability for all cell parameters under consideration. The increasing instability of V_{oc} and J_{sc} with increasing iron concentration reflects the change

in bulk lifetime at $\Delta n(V_{oc})$ and $\Delta n(J_{sc})$, respectively. Since this change is most prominent at $\Delta n(J_{sc})$, short circuit current is the most affected parameter in the presented case. The slightly increasing fill factor loss with increasing iron concentration reflects the different injection dependence of both the defects, Fe_i and FeB. Recombination via the Fe_i defect in p-type silicon is strongly injection dependent whereas the FeB defect only shows weak injection dependence.

From these results limits of tolerable iron concentration as a function of specific stability requirements can be deduced. For a relative instability of less than 2%, the maximum (dissolved) iron concentration should be below 7×10^{10} cm^{-3}, whereas the iron concentration should be below 3×10^{10} cm^{-3} for a relative instability of 1%. Note that these limits strictly apply only for the presented cell type.

It is interesting to note that metastability of cells with more cost effective concepts may still be lower than that discussed in this work although e.g. multicrystalline silicon material is used which exceeds the levels given above, provided the (stable) background lifetime is sufficiently low. The tolerable iron concentration in p-type solar cells is a strong function of material quality and cell concept. Obviously, n-type cells are advantageous with respect to this metastability since no iron–boron pairs are formed in this material.

High stability with respect to cell illumination is crucial for ensuring comparable results e.g. between flash and continuous light source IV-measurements. For the case that cells shall be used as references in industrial production even minor effects of iron induced metastability should be excluded preferably by minimizing the iron concentration alternatively by controlling the iron state during measurement. In order to select cells with proven electrical stability we propose a following simple procedure:

1. Dark storage of cell for approximately 12 h.
2. First IV-measurement with flash system.
3. 15 min illumination > 500 W/m².
4. Second IV-measurement with flash system and comparison with first measurement (ensure comparable cell temperature).
5. Dark storage of cell for approximately 12 h.
6. Third IV-measurement with flash system.

This procedure reveals any differences occurring due to iron-related metastability. The rule-of-thumb treatment parameters given are safety margins derived from practical experience. Both, the pairing as well as the splitting of FeB pairs are dependent on a variety of parameters like iron concentration, boron concentration, illumination intensity, background lifetime, and sample temperature. Depending on the specific parameter constellation shorter times for preparing the specific defect states may be sufficient. A detailed analysis of the pairing time can be found in [33]. The dissociation rate is discussed in [34–36]. A good overview of the interplay between pairing and dissociation is found in [37].

Comparison of the initial with the follow-up IV measurement reveals effective degradation during the illumination step. The third measurement quantifies the effect of metastability (in particular due
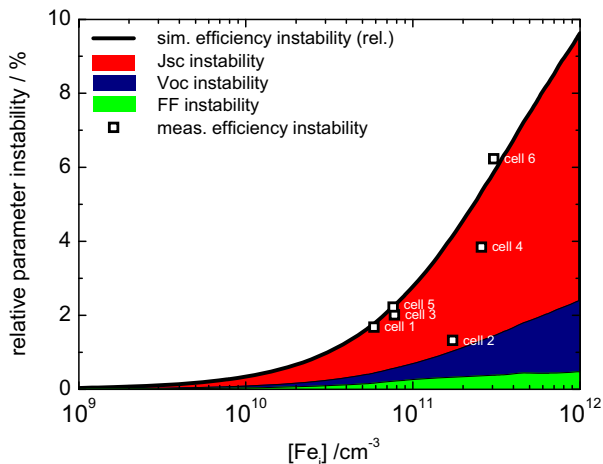
Fig. 4. Comparison of simulated relative cell parameter instabilities (FeB vs. Fe_i state) and experimental efficiency results. The PC1D simulations are based on a realistic cell model, including measured doping profiles, and assume carrier recombination by iron in its boron bound and interstitial form.

Table 1
Measured iron concentration, estimated iron concentration from V_{oc} (Eq. (7)) and cell parameters for cells shown in Fig. 4. The values have been taken in the FeB state. The values in parentheses represent the reduction after FeB pair splitting.

Cell	[Fe]$_{PLI}$ / (10^{10} cm^{-3})	[Fe]$_{Voc}$ / (10^{10} cm^{-3})	V_{oc} / mV (and instability)	J_{sc} / (mA cm^{-2}) (and instability)	FF / (%) (and instability)	η / (%) (and instability)
1	5.9	8.9	653.3 (−0.3)	38.4 (−0.4)	81.4 (−0.5)	20.4 (−0.3)
2	17.3	6.6	632.4 (−1.1)	38.3 (−0.4)	75.9 (−0.0)	18.4 (−0.2)
3	7.8	10.6	652.5 (−0.4)	38.2 (−0.5)	81.6 (−0.6)	20.3 (−0.4)
4	25.7	22.9	640.4 (−3.4)	37.8 (−1.0)	79.3 (−0.6)	19.2 (−0.7)
5	7.6	12.6	652.2 (−0.6)	38.3 (−0.5)	81.3 (−0.7)	20.3 (−0.5)
6	30.5	35.9	643.6 (−5.2)	37.6 (−1.5)	81.5 (−1.3)	19.7 (−1.2)

to iron). If the metastability is significant and can be traced back to the iron concentration in the solar cell, stable measurements can still be obtained if the iron state is carefully controlled. In this case, we suggest keeping the cell under illumination in order to ensure that dissolved iron is present only in its interstitial form.

5. Conclusion

A method for measuring the interstitial iron concentration in p-type silicon solar cells has been demonstrated which is based on dynamically calibrated photoluminescence imaging by modulated luminescence. With this method the measurement of iron is no longer restricted to wafers, thus allowing the influences of processing steps to be studied on cell level. The method is particularly useful for evaluating the influence of contact firing on the iron concentration as well as instabilities in the current–voltage characteristics due to metastable transformation of the iron point defect under illumination. The latter effect is demonstrated in this paper. The experimental findings agree well with PC1D based simulations of cell parameters. It is shown that even at rather low iron concentrations the metastability of the iron defect may yield significantly instable cell parameters in the case that iron is dominating carrier recombination. It is therefore recommended to control the illumination history of a p-type solar cell before measurement in order to measure in a well-defined iron defect state. A procedure is suggested for a safe quantification of iron-related metastability in a cell under test. In order to allow reproducible measurements of iron-affected solar cells we suggest keeping such cells under illumination for a sufficient amount of time in order to effectively split all iron boron pairs.

References

[1] A.A. Istratov, T. Buonassisi, R.J. McDonald, A.R. Smith, R. Schindler, J.A. Rand, J.P. Kalejs, E.R. Weber, Metal content of multicrystalline silicon for solar cells and its impact on minority carrier diffusion length, J. Appl. Phys. 94 (2003) 6552–6559.
[2] T. Buonassisi, A.A. Istratov, M.D. Pickett, M. Heuer, J.P. Kalejs, G. Hahn, M.A. Marcus, B. Lai, Z. Cai, S.M. Heald, T.F. Ciszek, R.F. Clark, D.W. Cunningham, A.M. Gabor, R. Jonczyk, S. Narayanan, E. Sauar, E.R. Weber, Chemical natures and distributions of metal impurities in multicrystalline silicon materials, Prog. Photovolt.: Res. Appl. 14 (2006) 513–531.
[3] S. Dubois, O. Palais, M. Pasquinelli, S. Martinuzzi, C. Jaussaud, N. Rondel, Influence of iron contamination on the performances of single-crystalline silicon solar cells: computed and experimental results, J. Appl. Phys. 110 (2006) 024510.
[4] S. Riepe, I. Reis, W. Kwapil, M.A. Falkenberg, J. Schön, H. Behnken, J. Bauer, D. Kreßner-Kiel, W. Seifert, W. Koch, Research on efficiency limiting defects and defect engineering in silicon solar cells—results of the German research cluster SolarFocus, Phys. Status Solidi C 8 (2011) 733–738.
[5] G. Coletti, Sensitivity of state-of-the-art and high efficiency crystalline silicon solar cells to metal impurities, Prog. Photovolt. 21 (2013) 1163–1170.
[6] J. Schmidt, B. Lim, D. Walter, K. Bothe, S. Gatz, T. Dullweber, P. Altermatt, Impurity-related limitations of next-generation industrial silicon solar cells, IEEE J. Photovolt. 3 (2013) 114–118.
[7] F. Schindler, B. Michl, J. Schön, W. Kwapil, W. Warta, M.C. Schubert, Solar cell efficiency losses due to impurities from the crucible in multicrystalline silicon, IEEE J. Photovolt. 4 (2014) 122–129.
[8] J. Schön, H. Habenicht, M.C. Schubert, W. Warta, Simulation of iron distribution after crystallization of mc silicon, Solid State Phenom. 862 (2009) 223.
[9] J. Schön, H. Habenicht, M. Schubert, W. Warta, Understanding the distribution of iron in multicrystalline silicon after emitter formation: theoretical model and experiments, J. Appl. Phys. 109 (2011) 063717.
[10] D.P. Fenning, J. Hofstetter, M.I. Bertoni, S. Hudelson, M. Rinio, J.-F. Lelièvre, B. Lai, C. Del Canizo, T. Buonassisi, Iron distribution in silicon after solar cell processing: synchrotron analysis and predictive modeling, Appl. Phys. Lett. 98 (2011) 162103.
[11] Lena Breitenstein, et al., Impact of Iron Surface Contamination on the Lifetime Degradation of Samples Passivated by Fired Al O/SiN Stacks. Photovoltaics, IEEE Journal of 3.3 (2013) 957–961.
[12] M. Kittler, W. Seifert, K. Schmalz, K. Tittelbach-Helmrich, Comparison of EBIC and DLTS measurements on boron-doped CZ slicon contaminated with iron, Phys. Status Solidi A 96 (1986) K133–K137.
[13] G. Zoth, W. Bergholz, A fast, preparation-free method to detect iron in silicon, J. Appl. Phys. 67 (1990) 6764–6771.
[14] D. Macdonald, J. Tan, T. Trupke, Imaging interstitial iron concentrations in boron-doped crystalline silicon unsing photoluminescence, J. Appl. Phys. 103 (2008) 073710.
[15] B. Mitchell, D. Macdonald, J. Schon, J.W. Weber, H. Wagner, T. Trupke, Imaging As-Grown Interstitial Iron Concentration on Boron-Doped Silicon Bricks via Spectral Photoluminescence, 2014.
[16] J.A. Giesecke, B. Michl, F. Schindler, M.C. Schubert, W. Warta, Minority carrier lifetime of silicon solar cells from quasi-steady-state photoluminescence, Sol. Energy Mater. Sol. Cells 95 (2011) 1979–1982.
[17] M.C. Schubert, H. Habenicht, W. Warta, Imaging of metastable defects in silicon, J. Photovolt. 1 (2011) 168–173.
[18] M.C. Schubert, J. Schön, A. Abdollahinia, B. Michl, W. Kwapil, F. Schindler, F. Heinz, M. Padilla, J.A. Giesecke, M. Breitwieser, Efficiency-limiting recombination in multicrystalline silicon solar cells, Solid State Phenom. 205 (2014) 110–117.
[19] J. Giesecke, M. Schubert, B. Michl, F. Schindler, W. Warta, Minority carrier lifetime imaging of silicon wafers calibrated by quasi-steady-state photoluminescence, Sol. Energy Mater. Sol. Cells (2010).
[20] K. Bothe, P. Pohl, J. Schmidt, T. Weber, P. Altermatt, B. Fischer, R. Brendel, Electroluminescence imaging as an in-line characterisation tool for solar cell production, in: Proceedings of the 21st European Photovoltaic Energy Conference, 2006, pp. 597–600.
[21] A.B. Sproul, Dimensionless solution of the equation describing the effect of surface recombination on carrier decay in semiconductors, J. Appl. Phys. 76 (1994) 2851–2854.
[22] V. Grivickas, D. Noreika, J.A. Tellesfen, Surface and Auger recombination in silicon wafers of high carrier density, Lith. Phys. J. 29 (1989) 48–53.
[23] J. Giesecke, Quantitative Recombination and Transport Properties in Silicon from Dynamic Luminescence, Springer International Publishing, Switzerland, 2014.
[24] A. Richter, S.W. Glunz, F. Werner, J. Schmidt, A. Cuevas, Improved quantitative description of Auger recombination in crystalline silicon, Phys. Rev. B 86 (2012) 165202.
[25] M.C. Schubert, M.J. Kerler, W. Warta, Influence of heterogeneous profiles in carrier density measurements with respect to iron concentration measurements in silicon, J. Appl. Phys. 105 (2009) 114903.
[26] R. Krain, S. Herlufsen, J. Schmidt, Internal gettering of iron in multicrystalline silicon at low temperature, Appl. Phys. Lett. 93 (2008) 152108.
[27] M.D. Pickett, T. Buonassisi, Iron point defect reduction in multicrystalline silicon solar cells, Appl. Phys. Lett. 92 (2008) 122103.
[28] M. Rinio, A. Yodyunyong, S. Keipert-Colberg, Y.P. Botchak Mouafi, D. Borchert, A. Montesdeoca-Santana, Improvement of multicrystalline silicon solar cells by a low temperature anneal after emitter diffusion, Prog. Photovolt. 19 (2011) 165–169.
[29] P. Karzel, A. Frey, S. Fritz, G. Hahn, Influence of hydrogen on interstitial iron concentration in multicrystalline silicon during annealing steps, J. Appl. Phys. 113 (2013) 114903.
[30] A. Liu, C. Sun, D. Macdonald, Hydrogen passivation of interstitial iron in boron-doped multicrystalline silicon during annealing, J. Appl. Phys. 116 (2014) 194902.
[31] A.A. Istratov, H. Hieslmair, E.R. Weber, Iron and its complexes in silicon, Appl. Phys. A: Mater. Sci. Process. 69 (1999) 13–44.
[32] D. Macdonald, A. Cuevas, J. Wong-Leung, Capture cross sections of the acceptor level of iron–boron pairs in p-type silicon by injection-level dependent lifetime measurements, J. Appl. Phys. 89 (2001) 7932–7939.
[33] D. Macdonald, T. Roth, P.N.K. Deenapranay, K. Bothe, P. Pohl, J. Schmidt, Formation rates of iron–acceptor pairs in crystalline silicon, J. Appl. Phys. 98 (2005) 083509.
[34] L. Kimerling, J. Benton, Electronically controlled reactions of interstitial iron in silicon, Phys. B+C 116 (1983) 297–300.
[35] L.J. Geerligs, D. Macdonald, Dynamics of light-induced FeB pair dissociation in crystalline silicon, Appl. Phys. Lett. 85 (2004) 5227–5229.
[36] L.J. Geerligs, G. Coletti, D. Macdonald, On accurate and quantitative measurements of iron-concentration in multicrystalline silicon by iron–boron pair dissociation, in: Proceedings of the 21st European Photovoltaic Solar Energy Conference, 2006, pp. 692–695.
[37] H. Habenicht, Charakterisierung leistungsmindernder Defekte und deren Umverteilung während der Herstellung von multikristallinen Silizium-Solarzellen, Verlag Dr. Hut, 2011.